J Mater Sci (2011) 46:6545–6555
DOI 10.1007/s10853-011-5601-x

Micromechanical multiscale model for alkali activation of fly ash and metakaolin

Vít Šmilauer · Petr Hlaváček · František Škvára · Rostislav Šulc · Lubomír Kopecký · Jiří Němeček

Received: 3 February 2011 / Accepted: 30 April 2011 / Published online: 21 May 2011

Abstract The process of alkali activation of fly ash and metakaolin is examined in the view of micromechanics. Elasticity is predicted via semi-analytical homogenization methods, using a combination of intrinsic elastic properties obtained from nanoindentation, evolving volume fractions and percolation theory. A new quantitative model for volume fraction is formulated, distinguishing the evolution of unreacted aluminosilicate material, solid gel particles of N-A-S-H gel, and open porosity, which is partially filled with the activator. The stiffening of N-A-S-H gel is modeled by increasing the fraction of solid gel particles. Their packing density and intrinsic elasticity differ in N-A-S-H gels synthesized from both activated materials. Percolation theory helps to address the quasi-solid transition at early ages and explains a long setting time and the beneficial effect of thermal curing. The low ability of N-A-S-H gel to bind water chemically explains the high porosity of Ca-deficient activated materials. Micromechanical analysis matches well the elastic experimental data during the activation and elucidates important stages in the formation of the microstructure.

V. Šmilauer (✉) · P. Hlaváček · R. Šulc · L. Kopecký · J. Němeček
Faculty of Civil Engineering, Czech Technical University in Prague, Thákurova 7, 166 29 Prague 6, Czech Republic
e-mail: vit.smilauer@fsv.cvut.cz

P. Hlaváček
e-mail: petr.hlavacek@fsv.cvut.cz

R. Šulc
e-mail: rostislav.sulc@fsv.cvut.cz

L. Kopecký
e-mail: kopecky@fsv.cvut.cz

J. Němeček
e-mail: jiri.nemecek@fsv.cvut.cz

F. Škvára
Department of Glass and Ceramics, Institute of Chemical Technology Prague, Technická 5, 166 28 Prague, Czech Republic
e-mail: frantisek.skvara@vscht.cz

Introduction

Reactions between strong alkaline liquids and solid aluminosilicate materials produce an inorganic binder, which is known as geopolymer, inorganic polymer, chemically bonded ceramics, or alkali-activated cement. The state-of-the art and historical achievements are comprehensively reviewed in several works [1−3]. It is worthy to note that the majority of fundamental research was carried out by chemists, who focused on atomistic and molecular scales using popular NMR or FTIR analyses. Another group of scientists tried to optimize the composition and curing process of activated materials, including fly ash [4−8].

The desire for a deeper understanding of alkali activation processes led researchers to various models. The first group of models focuses on the formation of a binder, emphasizing chemical and polycondensation processes during hardening [1, 9−11]. The second group describes reaction kinetics [11–13]. Notably, the model of Provis and van Deventer [14] aimed to capture eight ongoing reactions fitted with ten parameters. The third group describes the morphological evolution of the microstructure. For example, a descriptive model for alkali-activated fly ash captures general mechanisms independent of the activator composition or concentration [12]. All these models create a background for the micromechanical model assembled here.

To the best knowledge, no quantitative model describing the volumetric evolution of phases in a simple manner has been published. These first-order models are extremely important in characterizing the evolution of porosity, which is related to other properties such as elasticity or strength. Powers and Brownyards [15] created such a model for Portland cement, which was a breakthrough at that time and helped later to optimize the microstructure of ordinary concrete. A similar volumetric model for the alkali activation of fly ash and metakaolin is formulated here to fill the gap.

The application of mechanics on finer scales, known as micromechanics, brings a deeper insight into the formation of the microstructure and properties as has been demonstrated for Portland cement [16–18], concrete [19], or textile [20]. The focus here is given on multiscale elastic analysis, which is based on the definition of intrinsic elastic properties of constituents. These were previously identified by the grid nanoindentation technique [21]. The changes in volume fractions and connectedness of individual constituents on fine scales are projected to elasticity on a higher scale. The scale bridging explains the formation of N-A-S-H gel and the microstructure from another stand-point.

Materials and methods

Fly ash and metakaolin

Low-calcium fly ash of class F originates from the Opatovice thermal electric power plant, the Czech Republic. The specific Blaine surface is 210 m^2/ kg. The XRD Rietveld analysis yielded the composition of 70 vol.% amorphous phases, 24 vol.% mullite, and 6 vol.% quartz.

Metakaolin comes from České lupkové závody a.s., Nové Strašecí, the Czech Republic. Chemical compositions of both materials are given in Table 1 while Fig. 1 shows the particle size distributions.

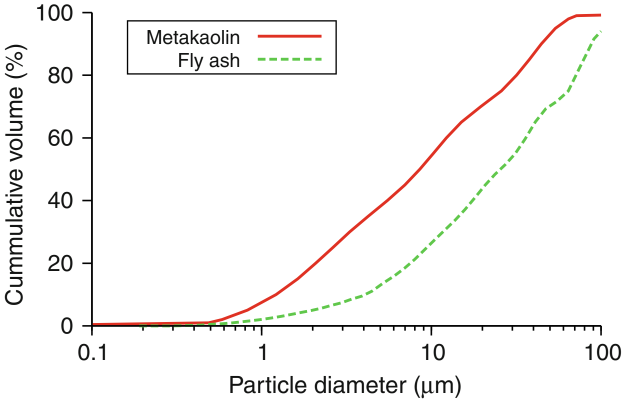

Fig. 1 Particle size distribution of fly ash and metakaolin

Alkali activator and curing

The activator was prepared from NaOH pellets, tap water, and sodium silicate in the form of water glass. Table 2 provides the ratii in the mixtures of fly ash and metakaolin. Note that metakaolin requires significantly more activator to maintain feasible workability. The compositions of both mixtures were previously optimized to yield high compressive strength [8]. The mixtures were stirred for 5 min and cast in either plastic ampules 26 mm in diameter and 45 mm in height or prisms 40 × 40 × 160 mm, gently vibrated for 5 min and sealed with a plastic foil. Ambient-cured samples were unmoulded after 10 days of hardening, after gaining sufficient strength, and kept in closed plastic bags. Heat-cured metakaolin samples were exposed to 80 °C for 12 h.

Table 1 The chemical composition of fly ash and metakaolin (wt%)

	SiO_2	Al_2O_3	Fe_2O_3	CaO	TiO_2	K_2O
Fly ash	51.9	32.8	6.3	2.7	1.89	2.12
Metakaolin	48.66	47.41	1.33	0.03	1.99	0.15

Table 2 Mixture composition. Mass oxide ratii for activators and activator-to-solid mass ratii

	Activator ratii		Activator-to-solid ratio (wt%)
	Na_2O/SiO_2 (−)	H_2O/Na_2O (−)	
Fly ash	0.881	3.925	0.531
Metakaolin	1.669	2.743	1.416

The 28-day compressive strength of heat-cured alkali-activated fly ash (AAFA) yields 84.14 ± 9.24 MPa, as determined from half-prisms 40 × 40 × 80 mm, and that of alkali-activated metakaolin (AAMK) 35.5 ± 1.20 MPa, obtained from 20 × 20 × 20 mm cubes.

Determination of open porosity

Cylindrical samples of a well-defined geometry (diameter ≈ 25 mm and thickness ≈ 5 mm) were dried out in an oven at 105 °C. The samples remained in the oven until the weight loss had stabilized, which took between 3 and 6 days. In addition, the He pycnometry provided skeletal densities of fly ash, metakaolin and activated mature samples. The open porosity was determined according to the following equation

$$\phi = \frac{\rho^{sk} - \rho^{b}}{\rho^{sk} - \rho^{im}}, \tag{1}$$

where ρ^{sk} represents the skeletal density, ρ^{b} is the bulk density, and ρ^{im} stands for the density of the intruding medium. For the determination of ρ^{sk}, crushed samples were dried at 105 °C for 12 h prior to MIP (Autopore III Micromeritics) and He pycnometry (Micromeritics AccuPyc 1330) tests. The ρ^{sk} value is biased with resolution limits of MIP from the top ($d \approx 120$ μm) and the He pycnometry resolution from the bottom ($d \approx 0.062$ nm). In the majority of cases, the intruding medium corresponded to air with $\rho^{im} \approx 0$ g/cm^3. Some samples were immersed into non-polar n-octane with $\rho^{im} = 0.70134$ g/cm^3 to check the penetration of larger molecules into smaller pores [22]. The open porosity was always determined as an average from three samples.

Continuum elastic micromechanics

Continuum micromechanics provides the framework in which elastic properties of heterogeneous microscale components are homogenized to the macroscale [23]. The analysis usually starts by defining a representative volume element (RVE), which identifies different components and their morphologies. Certain restrictions in terms of scale separation exist on the RVE size [23]; RVE must be substantially smaller than the macroscale body, which allows imposing homogeneous boundary conditions over RVE. This leads to a constant stress/strain field in individual microscale components of ellipsoidal shapes.

Effective elastic properties are obtained through averaging over the local contributions. Considering isotropic spherical inclusions perfectly bonded with a matrix leads to the estimation of effective bulk and shear moduli [23]

$$k_{\mathrm{eff}} = \frac{\sum_r f_r k_r \left[1 + \alpha_0\left(\frac{k_r}{k_0} - 1\right)\right]^{-1}}{\sum_r f_r \left[1 + \alpha_0\left(\frac{k_r}{k_0} - 1\right)\right]^{-1}}, \tag{2}$$

$$\mu_{\mathrm{eff}} = \frac{\sum_r f_r \mu_r \left[1 + \beta_0\left(\frac{\mu_r}{\mu_0} - 1\right)\right]^{-1}}{\sum_r f_r \left[1 + \beta_0\left(\frac{\mu_r}{\mu_0} - 1\right)\right]^{-1}}, \tag{3}$$

$$\alpha_0 = \frac{3k_0}{3k_0 + 4\mu_0}, \tag{4}$$

$$\beta_0 = \frac{6k_0 + 12\mu_0}{15k_0 + 20\mu_0}, \tag{5}$$

where f_r is the volume fraction of the rth phase, k_r its bulk modulus, and μ_r its shear modulus. A reference medium is described as the 0th phase.

Aligning k_0, μ_0 with a specific phase k_r, μ_r leads to the Mori–Tanaka method [24]. The reference medium creates a continuous matrix in which all inclusions are embedded. The self-consistent scheme of Budiansky, elaborated by Hill [25], is an implicit scheme for composites with a skeletal structure, where no dominant matrix exists. Now, the reference medium points back to the homogenized medium itself, which leads to $k_0 = k_{\mathrm{eff}}$ and $\mu_0 = \mu_{\mathrm{eff}}$ after several iterations.

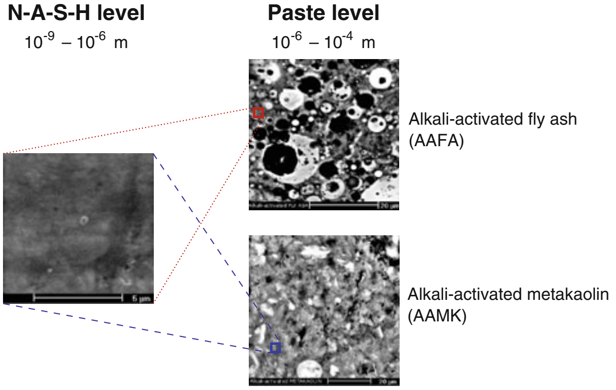

Fig. 2 Two levels in the multiscale analysis. The paste level displays two microstructures from alkali-activated fly ash and metakaolin

Levels of N-A-S-H gel and paste

The heterogeneity of alkali-activated materials is manifested on several length scales. For the analysis of alkali-activated pastes, the definition of two levels is appropriate. Figure 2 shows the level of N-A-S-H gel, which contains a poorly crystallized product from a low calcium, alkali-activated material [4]. The paste level contains remnants of activated material, a part of the open porosity partially filled with an activator and the N-A-S-H gel.

Results and discussion

Figure 3 shows three characteristic BSE images of mature AAFA and AAMK samples.

Degree of reaction

The degree of reaction, abbreviated as DoR, is defined as the amount of activated material consumed during the alkali activation process. In the activated material, reactive vitreous components are not differentiated from slowly reacting crystalline phases, hence DoR is always lower than one. The direct simulation of the DoR evolution in time, or reaction kinetics, is beyond the capabilities of presented models. Instead, the evolution of DoR in AAFA is taken from experimental data of Chen et al. [13], who measured the DoR progress on AAFA samples activated with 7.5 M KOH solution. The extent of DoR was determined by the HCl acid attack. Similar kinetic results were observed on calorimetric data, revealing that the activator/fly ash ratio is insignificant for the DoR evolution and that

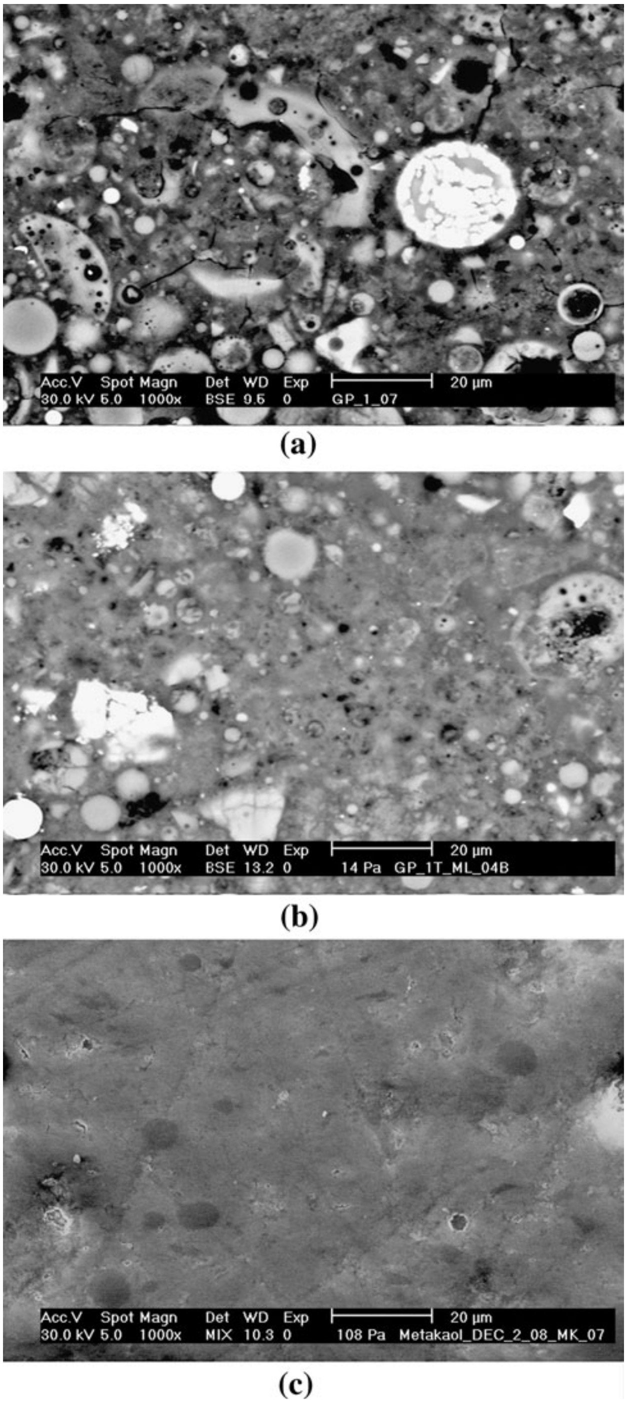

Fig. 3 BSE images of matured AAFA and AAMK samples used further. **a** Ambient-cured fly ash for 11 months at ≈25 °C. **b** Heat-cured fly ash at 80 °C for 12 h. **c** Heat-cured metakaolin at 80 °C for 12 h

a maximum reaction rate occurs at 8–10 min after the contact, substantially reduced after 2 h at elevated temperatures [26].

The Arrhenius equation is utilized to recalculate DoR for various curing temperatures

$$\tau_e(T_0) = \tau(T)\exp\left[\frac{E_a}{R}\left(\frac{1}{T_0} - \frac{1}{T}\right)\right], \tag{6}$$

where T is an arbitrary constant temperature, T_0 is the reference temperature, R is the universal gas constant (8.314 J/mol K) and E_a is the apparent activation energy. The activation energy was found as 86.2 kJ/mol via isothermal calorimetry for activated AAFA using 8 M NaOH [8] which fits within 60–102 kJ/mol [13], although lower energies such as 31.5 ± 6 kJ/mol were reported for a different system of metakaolin and potassium activator [27]. Figure 4 shows the DoR evolution at 25 °C, recalculated from the data presented in [13] for temperatures of 20–75 °C with the help of Eq. 6. Also, the data from Fig. 4 were fitted using the Levenberg–Marquardt algorithm to the function

$$\mathrm{DoR} = \frac{0.8}{1 + (0.17 - 0.17\ln(t/10^4))^{4.477}}, \quad t \le 10^4 \text{ days}, \; R^2 = 0.954, \tag{7}$$

where t stands for an activation time in days at a temperature of 25 °C. Similar results for the evolution of DoR are available elsewhere [11, 12].

AAMK reacts much faster than fly ash and the kinetics was not monitored. Deduction from nanoindentation data provided DoR for mature AAMK samples as described in the following subsection.

Volumetric model for alkali activation

The volumetric model for the alkali activation process presents a stepping stone in micromechanical analysis.

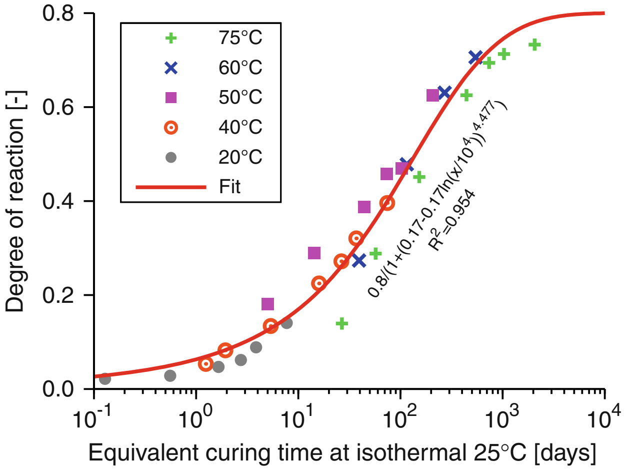

Fig. 4 Progress of DoR for alkali-activated fly ash by 7.5 M KOH obtained by time scaling according to Eq. 6. Here, the evolution of DoR is showed for a reference temperature of 25 °C. Original data [13] were gathered at isothermal temperatures of 20–75 °C. Activation energy considered is 86.2 kJ/mol

Much inspiration has been gathered from Portland cement-based systems, through famous research carried out by Powers and Brownyard [15]. Three assumptions underline the presented volumetric model:

1. No change in volume occurs after initial setting. The volumetric balance of all liquid and solid phases is maintained at any time. Although alkali-activated pastes exhibit high autogenous shrinkage, the effect in volume reduction is low. Rodríguez et al. [28] report high autogenous shrinkage, 8000 μstrain after 35 days of AAMK paste curing. This corresponds to 2.4% decrease in volume. Strnad [29] reports 4240 μstrain after 28 days of AAFA paste ambient curing. To the best knowledge, chemical shrinkage was never reported for AAMK or AAFA; the model makes no difference between filled and empty capillary pores.
2. The model uses only the DoR as the independent variable. Such a simplification neglects separate contributions of dissolution and polymerization of N-A-S-H gel, as previously noted [30]. More precise calculations would determine DoR from formed gel, instead of from dissolved material [3, p 123].
3. The whole activator is treated in the form of evaporable water, disregarding the solid part remaining after drying.

The volumetric model for AAFA or AAMK is expressed with a set of linear equations. They contain no time and depend on initial volumetric fractions and DoR only

$$f_{\mathrm{FA,MK}}^{\mathrm{Skel}}(\mathrm{DoR}) = \mathrm{f}_{\mathrm{FA,MK}}^{\mathrm{Skel}}(0^{+})[1-\mathrm{DoR}], \tag{8}$$

$$f_{\mathrm{SGP}}(\mathrm{DoR}) = \left[\mathrm{f}_{\mathrm{FA,MK}}^{\mathrm{Skel}}(0^{+})+\alpha\right]\mathrm{DoR}, \tag{9}$$

$$f_{\mathrm{FA,MK}}^{\mathrm{Voids}}(\mathrm{DoR}) = \mathrm{f}_{\mathrm{FA,MK}}^{\mathrm{Voids}}(0^{+})-\beta\mathrm{DoR}, \mathrm{f}_{\mathrm{FA,MK}}^{\mathrm{Voids}}(\mathrm{DoR})\geq 0, \tag{10}$$

$$f_{\mathrm{OP}}(\mathrm{DoR}) = 1-\mathrm{f}_{\mathrm{FA,MK}}^{\mathrm{Voids}}(\mathrm{DoR})-\mathrm{f}_{\mathrm{FA,MK}}^{\mathrm{Skel}}(0^{+})-\alpha\mathrm{DoR}. \tag{11}$$

The meaning of the symbols is explained on the system of activated fly ash first, see Fig. 5a for graphical representation. $f_{\mathrm{FA}}^{\mathrm{Skel}}(\mathrm{DoR})$ represents the skeletal volume fraction of unreacted fly ash. The voids persisting in unreacted fly ash are quantified with $f_{\mathrm{FA}}^{\mathrm{Voids}}(\mathrm{DoR})$. It must be noted that the activator efficiently destroys a thin shell of plerospheres within a few minutes and opens the voids, which is denoted as time 0^{+}. This is manifested by a partial loss of workability and heat release in isothermal calorimetry. $f_{\mathrm{FA}}^{\mathrm{Voids}}(0^{+})$ was determined from the combination of the known skeletal density of fly ash, the known density of activating solution and the measured volume, and the weight of the mixture immediately after mixing.

f_{SGP} represents the volume fraction of solid gel particles. The term N-A-S-H gel is intentionally not used since it is defined on a higher scale as a combination of solid gel particles and a part of open porosity.

f_{OP} represents the volume of open porosity, which equals the maximum volume occupied with evaporable water. The activator fills up the major part of open porosity during the activation.

Five parameters from Eqs. 8–11 have to be determined from a known composition. Table 3 summarizes densities, initial volume fractions and parameters α, β. The parameter

Table 3 Fitted parameters for the volumetric model of alkali activation

Parameter	AAFA	AAMK
Skeletal density of activated material (g/cm^3)[a]	2.070	2.372
Density of activator (g/cm^3)	1.545	1.477
Bulk density of paste (g/cm^3)[bc]	1.752	1.694
$f_{\mathrm{FA,MK}}^{\mathrm{Skel}}(0^{+})$	0.581	0.296
$f_{\mathrm{OP}}(0^{+})$	0.355	0.672
$f_{\mathrm{FA,MK}}^{\mathrm{Voids}}(0^{+})$	0.064	0.032
Parameter α	0.224	0.294
Parameter β	0.152	0.064

[a] Determined from He pycnometry

[b] Determined from measured geometry and sample mass

[c] Including entrapped air

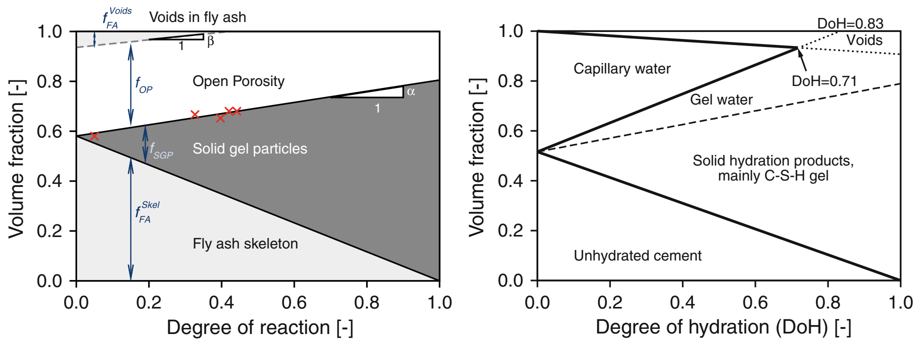

(a) **(b)**

Fig. 5 The newly created volumetric model for alkali activation of fly ash and comparison to the Powers model for Portland cement. Measured open porosity is marked with crosses, parameters are summarized in Table 3. **a** Activated fly ash. **b** Portland cement at w/c = 0.3

β was obtained from porosity calculations using two intruding media according to Eq. 1. Here, the method of *n*-octan intrusion [22] yielded generally lower values than by water evaporation. Both porosities merged when DoR $\geq$ 0.42, which leads to $\beta = 0.064/0.42 = 0.152$.

Figure 5b illustrates the fact that the Powers model for ordinary Portland cement paste yields a similar evolution of volume fractions as Fig. 5a. The major difference lies in gel water (occupying gel porosity under saturated conditions), associated with a characteristic 28% porosity of C-S-H [31]. Characteristic porosity of N-A-S-H gel is an invalid hypothesis as will be explained in "Elastic downscaling to a solid gel particle" section.

AAMK contains a much larger amount of open porosity, see Fig. 6. The AAMK bulk density of 1.694 g/cm^3, see Table 3, corresponds well with the experiments of Duxson et al. [32], who reported 1.68–1.80 g/cm^3. The degree of reaction of mature samples, cured at 80 °C for 12 h, was determined from a histogram of indentation moduli [21]. Unreacted metakaolin corresponded to 2.8% of all solids by volume. Since nanoindentation does not "see" pores and open porosity was measured as 0.4263, DoR $= 1 - (1 - 0.4263) \cdot 0.028/0.296 = 0.946$ for a mature AAMK sample.

The pore size distribution obtained from MIP and He pycnometry is depicted in Fig. 7 for mature samples. Also, it is shown that matured ordinary Portland cement paste with a water-to-cement ratio of 0.5 yields lower total porosity than presented activated materials. Note that ambient/heat curing of fly ash yields the same amount of open porosity but ambient curing contains more coarse pores. A different pore distribution also becomes obvious from Fig. 3.

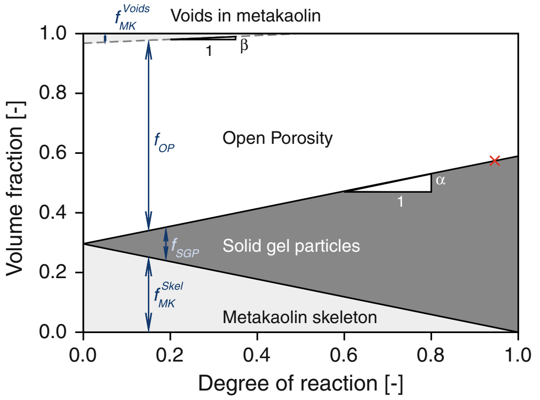

Fig. 6 The volumetric model for alkali activation of metakaolin. Measured open porosity is marked with the *cross*

The porosity results for AAFA are higher than those reported by Kovalchuk et al. [7], who found total porosity of activated fly ash, class F, between 15 and 20%, depending on the curing setup at a temperature of 95 °C. They also noted that larger pores emerge under dry curing due to the evaporation of water and shrinkage of N-A-S-H gel.

Elastic downscaling to a solid gel particle

Elastic properties of mature N-A-S-H gel were previously obtained via grid nanoindentation from about 700 locations [21]. The mean Young's modulus was unambiguously found in the range of 17.03–17.72 GPa, covering activated fly ash and metakaolin, cured under ambient or heat conditions. The indentation depth was approximately 300 nm, which reflects a part of open porosity, see Figs. 3 and 7.

Any sol–gel system (C-(A)-S-H, N-A-S-H) consists of solid particles dispersed in a liquid [33]. Sol–gel is far from equilibrium and solid particles may aggregate into clusters. If a condensation reaction in the system exists and is irreversible, more and more solid particles appear in the system and grow into fractals [33]. The linking of clusters continues until they reach a percolation threshold signalized by a sudden change of many properties such as elasticity.

It is worthy to mention that C-S-H is not a true gel but a precipitate, signalized by the presence of capillary pores and the appearance mainly around cement grains. A reversible condensation reaction dominates the C-S-H solidification [33]. Another consequence of reversibility is a constant 28% porosity of the C-S-H gel, irrespective of its origin [15]. The constant porosity allowed considering the C-S-H gel as one phase from a micromechanical perspective; a building block intermixed with porosity at a constant fraction [34, 35].

Fig. 7 Cumulative pore volume for alkali-activated materials and Portland paste cured at 60 °C for 3 months. An *asterisk* denotes the total volume using also skeletal density from He pycnometry

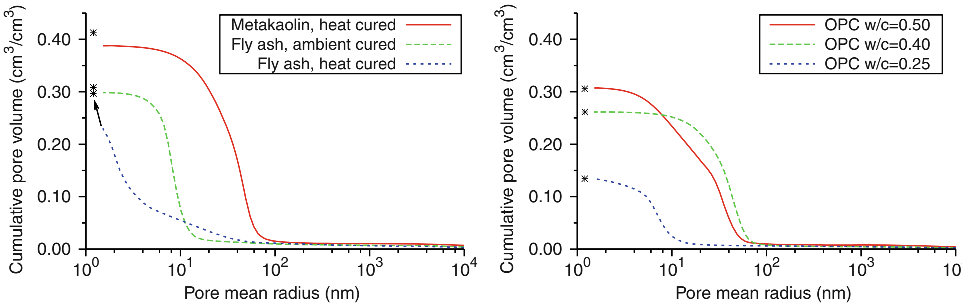

(a) (b)

On the other hand, N-A-S-H is a true gel, which rather fills out all available volume and does not form only on the surface of activated material. The gel syneresis has been observed many times in alkali-activated materials; excessive shrinkage accompanied with strong sample disintegration might occur under sealed conditions [6, 29, 36]. Due to a true gel nature, no constant gel porosity exists, as in the case of C-S-H, and the micromechanical response needs to be determined from solid gel particles at the N-A-S-H level.

Two micromechanical parameters need to be identified for mature materials; the modulus of a fictitious solid gel particle and a fraction of open porosity which is associated to the N-A-S-H level. The latter is captured with the parameter $0 \leq \gamma \leq 1$, where 1 means a complete assignment of the open porosity to the N-A-S-H level. These two unknowns are unambiguously determined from nanoindentation moduli and macroscopic moduli. Table 4 summarizes data for mature AAFA and AAMK materials at the time of nanoindentation. In the case of AAFA, 98 days of ambient curing corresponds to DoR = 0.440 as determined from Eq. 7.

First, the parameter γ was determined from the known intrinsic properties in Table 5 and using homogenization via the self-consistent scheme at the paste level. The scheme is suitable especially for AAFA, where the volume fractions are roughly equal $f_{\mathrm{SGP}} \approx f_{\mathrm{OP}} \approx f^{\mathrm{Skel}}{}_{\mathrm{FA}}$ at DoR = 0.44 and no dominant matrix can be distinguished. While practically all open porosity remained on the N-A-S-H level for AAFA, less than one third remained in the case of AAMK. Such a result is consistent with Fig. 7, showing coarser porosity for AAMK.

Table 4 Parameters of mature activated materials at the time of indentation

Parameter	AAFA[a]	AAMK[d]
DoR	0.440	0.946
$f_{\mathrm{FA,MK}}^{\mathrm{Skel}}$	0.325	0.016
f_{SGP}	0.354	0.558
f_{OP}	0.321	0.426
$f_{\mathrm{FA,MK}}^{\mathrm{Voids}}$	0.000	0.000
γ	1.000	0.306
Normalized f_{SGP} on N-A-S-H level	0.525	0.811
Normalized f_{OP} on N-A-S-H level	0.475	0.189
E_{SGP}, downscaled (GPa)	48.160	25.480
E_{gel}, experiment (GPa)	17.72 ± 3.75[ac]	17.72 ± 4.43[cd]
E_{gel}, upscaled (GPa)	17.72	17.72
E_{paste}, experiment (GPa)	32.05 ± 0.90[ab]	7.369 ± 0.517[d]
E_{paste}, upscaled (GPa)	28.279	7.369

[a] Ambient cured

[b] Interpolated

[c] Němeček et al. [21]

[d] Heat-cured

Table 5 Intrinsic elastic properties used in homogenization models

Material	Young's modulus (GPa)	Poisson's ratio
Fly ash skeleton	105[a]	0.2
Metakaolin skeleton	43.91[b]	0.2
N-A-S-H gel	17.72[b]	0.2
Open pores	0.001	0.001

Note Indentation moduli of fly ash and metakaolin skeletons underestimate their true stiffness; displacement under the indenter tip is biased with the deformation of compliant N-A-S-H gel surrounding the particles. The value 105 GPa for the fly ash skeleton assumes an average particle diameter 20–45 μm and the parallel arrangement of glass, mullite and quartz [37]. Indeed, the modulus from nanoindentation gives only 79.65 GPa [21]

[a] Matsunaga et al. [37]

[b] Němeček et al. [21]

Second, the downscaling from N-A-S-H gel to the solid gel particle was executed with the help of the Mori–Tanaka method. The self-consistent scheme, as an alternative, could not be applied. The reason is a high fraction of water-filled pores, which are close to the percolation threshold of the scheme. Unfortunately, the Young moduli 48.160 and 25.480 GPa show that no common solid gel particle exists for AAFA and AAMK.

The micromechanical analysis shows that the gel synthesized from AAMK is richer in solid gel particles which are also twice as compliant, compared to the gel from AAFA. This does not necessarily imply a different chemical composition of both gels, although small differences in the aluminum coordination and ^{29}Si NMR spectra were reported [1, 38]. In addition to chemical analysis, elastic modulus is a volumetric integral quantity, which also reflects the interaction between gel particles, their arrangement, organization, spacing, bonds, or rarefaction/compaction [39]. The metastable gel composition in activated materials is known to vary with an activator or the curing procedure. For example, a higher content of soluble Si in the system creates denser gel in AAMK [32]. Note that the activators were optimized to yield high compressive strength and they have different compositions.

Another factor yielding different elasticity of solid gel particles may arise from assumptions in homogenization methods, particularly perfect bonds among phases and ergodicity. The Mori–Tanaka scheme assumes matrix-inclusion morphology with a uniform distribution of solid gel particles in space. When a cluster-like assemblage with percolation characteristics dominates the morphology, several solid gel particles remain unconnected. Homogenization methods smear such an effect which leads to apparently softer inclusion. Other experimental methods

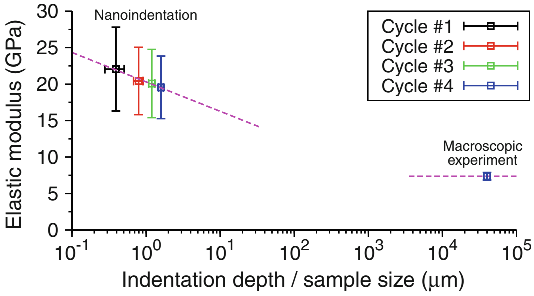

Fig. 8 Continuous porosity distribution of AAMK leads to the decrease of elastic moduli with the sample volume

are needed to support these indirect indications of different N-A-S-H gel nanostructures.

A continuous distribution of porosity breaks the condition of scale separation [23]. Figure 8 illustrates such a fact via a 10 × 12 nanoindentation grid on mature AAMK with a spacing of 30 μm and varying indenter's depth. The first cycle of the indenter penetrates roughly 400 nm into the material, is unloaded and continues on the same spot up to 800, 1200, and 1600 nm. It is worthy to note that the indenter does not "see" voids on the surface and measures, in fact, the underlying solid material. Larger indents take more material into account and converge to the macroscopic modulus obtained on prisms 40 × 40 × 160 mm.

Notes on drying shrinkage

High autogenous shrinkage of alkali-activated concretes and pastes was noted under ambient-curing temperature [6, 28, 29, 36]. Since the samples were not mechanically restrained before the tests, no stress had evolved and no cracking had occurred. Autogenous shrinkage, whatever magnitude it had, proceeded freely without any induction of damage. No microcracks were observed on the specimens, which is also demonstrated in Fig. 9 with a perfect linear behavior on mature AAMK during cyclic loading.

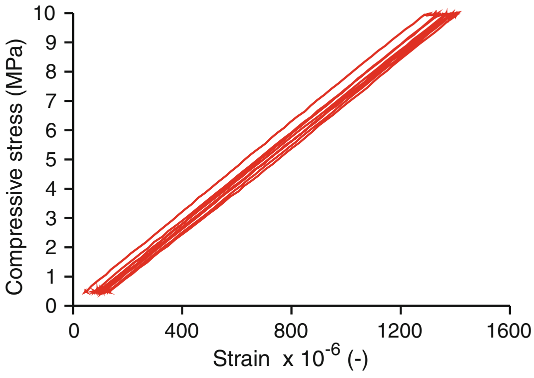

Fig. 9 A characteristic stress–strain plot of a AAMK prism 40 × 40 × 160 mm loaded uniaxially. Five loading/unloading cycles are shown, testifying linear dependence

Drying shrinkage is the well-known phenomenon for porous materials, where alkali-activated materials are of no exception. Exposing AAFA and AAMK samples to RH ≈ 30% led to the introduction of moisture gradients, shrinkage, and consequent tensile stress. Figure 10 demonstrates this fact on alkali-activated pastes after the exposure of approximately 1 year to RH ≈ 30%. These ambient-cured AAFA samples exhibit crack formation and propagation while the heat-cured AAMK sample seems to be free of macrocracks.

Introducing aggregates into shrinking alkali-activated material efficiently mitigates the macrocrack formation and the overall shrinkage [40, p 430]. The results have indicated that compressive strength steadily increases over years without any notion of the deterioration or crack formation on AAFA concrete under RH ≈ 30% [8].

Elasticity evolution during alkali activation process

The combination of a volumetric model, intrinsic elastic properties and a two-scale homogenization allows us to compute the evolution of elasticity during the alkali activation process. The upscaling starts from the solid gel particle and the moduli are matched exactly at the N-A-S-H level, see Fig. 11. It is evident from the paste moduli that a certain DoR must proceed before the gel interconnects the unreacted material. Introducing lower and upper percolation bounds, $\mathrm{DoR}_{\mathrm{LB}}$, $\mathrm{DoR}_{\mathrm{UB}}$, a solid percolation fraction is determined as

$$p = \frac{\mathrm{DoR} - \mathrm{DoR}_{\mathrm{LB}}}{\mathrm{DoR}_{\mathrm{UB}} - \mathrm{DoR}_{\mathrm{LB}}}, \quad 0 \leq p \leq 1. \tag{12}$$

The elastic moduli from the N-A-S-H level are multiplied with p. From the macroscale tests, the bounds were

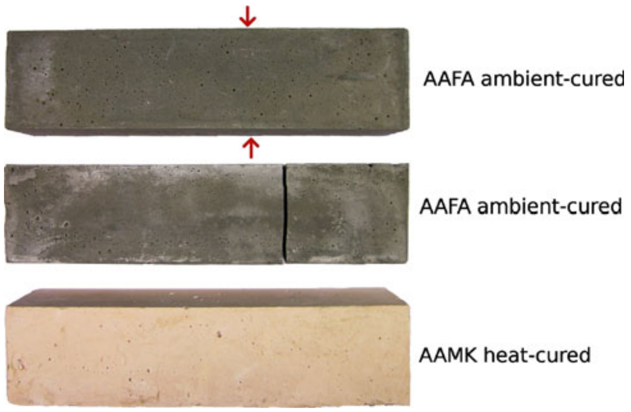

Fig. 10 Drying shrinkage on ambient-cured AAFA and heat-cured AAMK samples when exposed to RH ≈ 30%. An *arrow* on the prism 40 × 40 × 160 mm shows a visible microcrack which will propagate and later disintegrate the AAFA sample. Efflorescence on the surface originates from carbonation of excessive alkalies, which are carried to the surface in a moisture-gradient environment

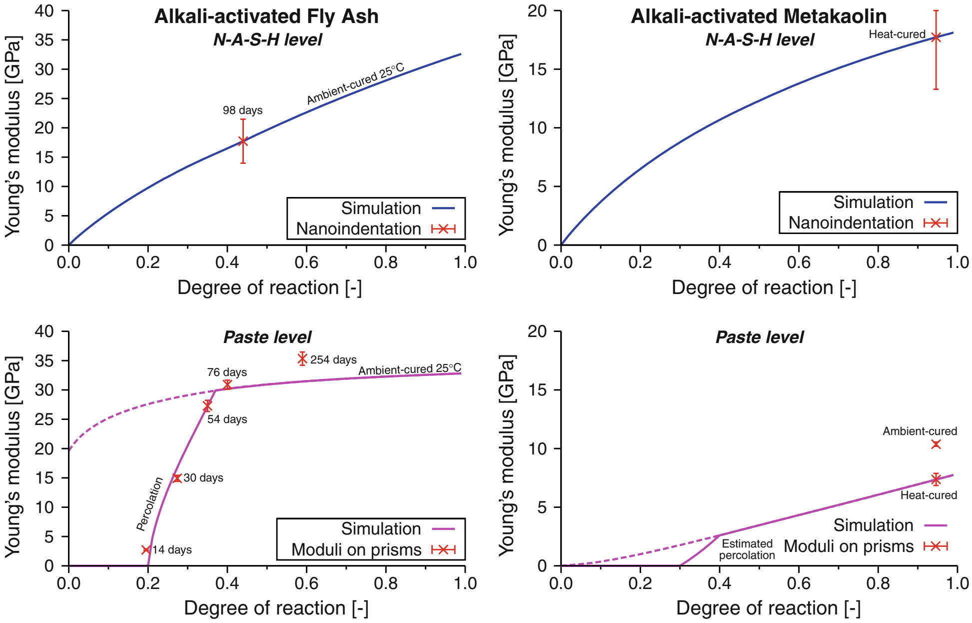

Fig. 11 Simulated and measured Young's moduli on the levels of N-A-S-H gel and paste, for both AAFA and AAMK materials. *Dashed lines* disregard solid percolation

fitted to $\mathrm{DoR}_{\mathrm{LB}} = 0.20$, $\mathrm{DoR}_{\mathrm{UB}} = 0.37$ for AAFA and nicely demonstrate a steep evolution of elasticity in this region. Both bounds will be a function of the activator content since more solid gel particles are needed to bridge a larger gap among unreacted particles. This is analogous to Portland cements, where more hydration is needed for a higher water-to-cement ratio to achieve the percolation threshold of solids [41]. Dashed lines show the results under the assumption of perfect bonding among the phases.

Since finite elasticity is aligned with a solid material, the evolution of compressive/tensile strength follows the same pattern. This was demonstrated by Chen et al. [42], who found a steep gain of compressive strenght when the material passed DoR between 0.15 and 0.35, depending on KOH molarity. The percolation thresholds are close to their values, which supports the view of dominating percolation mechanisms in the N-A-S-H gel formation.

Figure 11 also captures statistics; nanoindentation results are gathered from 500–700 indents [21] and cyclic load was applied on three prisms 40 × 40 × 160 mm. The paste modulus of AAFA at 254 days is underestimated by 13%. The main reason probably lies in selective dissolution of fly ash, where remaining mullite has a high Young modulus of 230 GPa [37] and boosts the stiffness of the fly ash skeleton considerably. Another reason could be the assumptions underlying continuum micromechanical methods; a strong interaction among fly ash particles violates the homogeneous strain field around them. Also, N-A-S-H gel undergoes aging and rearrangement, changing the porosity distribution, the parameter γ, and possibly the intrinsic elasticity of a fictitious solid gel particle.

Figure 11 also provides the evolution of moduli for AAMK with experimental data on mature samples. Lower and upper percolation bounds were estimated. The heat-cured mature AAMK yielded a lower modulus than the ambient-cured counterpart, which could be explained micromechanically by changing the intrinsic elasticity of the solid gel particle or the parameter γ. Also, accelerated aging of activated metakaolin at elevated temperatures proved the gel transformation to Na-P1 zeolites [3, p 148], which would affect elasticity as well.

The elastic moduli for mature AAMK, found in the range of 7.37–10.37 GPa, correspond well with literature data; 2.5–5.5 GPa [32], 1–6 GPa [43], and up to 9.22 GPa [44]. On the contrary, the moduli for AAFA pastes are scarce in literature. Our colleague reported a dynamic modulus of 23.02 GPa for the AAFA paste after 308 days of curing at $\approx$ 22 °C [29].

More data exist for AAFA concrete; dynamic modulus of 22.15 GPa (also measured tangent static modulus of the same specimen 21.0 GPa) after 124 days of curing at $\approx$22 °C, attaining 24.6 GPa after 482 days [29]. Wongpa et al. [36] obtained chord moduli of 5.6–16.9 GPa on concrete with substantial cracks and Wallah and Rangan [6] reported tangent instantaneous moduli of 21.1–29.6 GPa for concrete. Considering concrete with 30 GPa, aggregate's moduli of 40 GPa and their volume fraction of 0.85, the AAFA paste should have 9.1 GPa using the Mori–Tanaka method. We hypothesize that such low moduli for the AAFA paste are caused by microcracks in the AAFA paste, which are unable to close up contrary to self-healing effects and carbonation in Portland-based systems.

Certain comparison also exists with the unpublished previous experiments, which did not prevent water evaporation by mould covering and sealing the samples during curing. Such measurements indicated much lower tangent moduli of mature AAFA pastes; 6.1 ± 1.8 GPa for ambient-cured and 8.35 ± 1.7 GPa, 11.4 ± 0.2 GPa for heat-cured specimens with similar compositions. The majority of previous AAFA pastes developed visible cracks on the surface, which apparently strongly reduced the specimen's moduli.

Relation to selected alkali activation models

The presented multiscale model shows no significant contradictions to existing models of alkali activation, especially due to a different approach and stand-point. The current model contributes to the chemically based models by treating the gel as an agglomeration of solid gel particles. Such a representation is advantageous in the micromechanical model, however, the shape of a solid gel particle can be almost arbitrary, intermixed with nanoporosity. The model of Barbosa et al. perfectly fits for the nanostructure of N-A-S-H gel [45].

Although N-A-S-H gels, originating from AAFA or AAMK, yield similar stiffnesses on the submicrometer scale [21], their nano-particulate structure appears to be micromechanically different. The N-A-S-H level shows significant variations in stiffness for a fictitious solid gel particle, which could be linked to gelation, reorganization and polymerization steps identified in a conceptual model of Duxson et al. [1] or Criado et al. [11]. More research is needed to validate the hypothesis about the same N-A-S-H gel nanostructure in AAFA and AAMK materials, even though TEM samples under high vacuum revealed very similar N-A-S-H morphologies [1].

A descriptive model of alkali activation of fly ash [12] reveals more detailed reaction mechanisms than quantified here. N-A-S-H gel, as the main reaction product, is not distributed only around fly ash as a precipitate but also fills capillary porosity as a true gel. Good adhesion to the majority of materials is a consequence of such gel formation [3]. Changing the reaction orders due to the deposition of reaction products [13] and depletion of the alkali potential remains unaddressed in the presented model and the whole kinetics must be provided externally.

Low chemical binding of capillary water to N-A-S-H gel testifies that water plays a major role for the dissolution and transport of dissolved glasses, but not to be consumed substantially [1]. Gelation, reorganization, and polymerization return water back to the system. The excess of water during curing is not beneficial as opposed to Portland-based systems [7]. Dry curing was found to remove water and to stop reactions prematurely [7]. Introducing Ca-rich materials into the system would combine Figs. 5a,b and would reduce capillary porosity. It is known that high alkalinity hinders the dissolution of $Ca(OH)_2$ and prevents, to some extent, the formation of C-(A)-S-H gels [3, p 84].

Conclusions

The application of elastic micromechanics with the volumetric model of alkali activation leads to the following conclusions:

1. Water is consumed only marginally during the alkali activation process in both AAFA and AAMK systems. For this reason, the volume fraction of a liquid activator governs the final open porosity. This is critical especially for activated metakaolin, where large quantities of the activator are needed for proper workability.
2. Introducing Ca in the system would be beneficial for possible water binding to C-(A)-S-H gels thus reducing capillary porosity.
3. Micromechanical analysis revealed elastic differences in the N-A-S-H gel composition on the nanometer scale. A fictitious solid gel particle in AAMK is almost twice as compliant as in the AAFA counterpart. Also, AAMK contains almost three times less porosity associated with the N-A-S-H level than AAFA. Commonly used methods, such as NMR, FTIR, or XRD, may provide only indirect evidence. This topic needs more research with consequences to stability and durability of AAFA and AAMK materials.
4. Percolation plays a significant role during the alkali activation process. A slow reaction kinetics at ambient temperature combined with a high percolation threshold implies slow hardening especially for AAFA.
5. The results testify that curing temperature has a small effect on the total open porosity or the micromechanical properties of mature AAFA [21]. However, ambient curing creates more coarse pores which is probably related to N-A-S-H gel's syneresis.
6. The presented model for alkali activation is general enough to accommodate different activated materials, various compositions of the activator and mixture proportions. Recalibration and kinetic monitoring must be executed prior to modeling.

Acknowledgements This research was supported by the Czech Science Foundation under the grant GAP104/10/2344, GA103/09/1748 and MSM 6046137302. M. Vokáč from Klokner Institute, CTU in Prague is greatly acknowledged for conducting precise measurements of elastic moduli.

References

1. Duxson P, Fernández-Jiménez A, Provis JL, Lukey GC, Palomo A, van Deventer JSJ (2007) J Mater Sci 42(9):2917. doi:10.1007/s10853-006-0637-z
2. Pacheco-Torgal F, Castro-Gomes J, Jalali S (2008) Constr Build Mater 22(7):1305
3. van Deventer JSJ (eds) (2009) Geopolymers: structures, processing, properties and industrial applications, 1st edn. Woodhead Publishing Ltd, Cambridge
4. Fernández-Jiménez A, Palomo A (2005) Cem Concr Res 35:1984
5. Hardjito D, Rangan BV (2005) Research report gc 1. Faculty of Engineering, Curtin University of Technology, Perth
6. Wallah SE, Rangan BV (2006) Research Report GC 2. Curtin University of Technology, Perth
7. Kovalchuk G, Fernandez-Jimenez A, Palomo A (2007) Fuel 86(3):315
8. Škvára F, Kopecký L, Šmilauer V, Bittnar Z (2009) J Hazard Mater 168:711
9. Davidovits J (2001) In: Metha PK (ed) Concrete technology, past, present and future, Proceedings of V. Mohan Malhotra Symposium, ACI, p 383
10. van Jaarsveld JGS, van Deventer JSJ, Lorenzen L (1997) Miner Eng 10(7):659
11. Criado M, Fernández-Jiménez A, Palomo A (2010) Fuel 89(11):3185
12. Fernández-Jiménez A, Palomo A, Criado M (2004) Cem Concr Res 35:1204
13. Chen C, Gong W, Lutze W, Pegg I, Zhai J (2011) J Mater Sci 46(3):590. doi:10.1007/s10853-010-4997-z
14. Provis JL, van Deventer JSJ (2007) Chem Eng Sci 62:2309
15. Powers TC, Brownyards TL (1948) Studies of physical properties of hardened portland cement paste. Bulletin 22, Research Laboratories of the Portland Cement Association, Chicago
16. Bernard O, Ulm FJ, Lemarchand E (2003) Cem Concr Res 33(9):1293
17. Šmilauer V, Bittnar Z (2006) Cem Concr Res 36(9):1708
18. Pichler C, Lackner R, Mang HA (2007) Eng Fract Mech 74:34
19. Grassl P, Jirásek M (2010) Int J Solids Struct 47(7–8):957
20. Šejnoha M, Zeman J (2008) Int J Eng Sci 46(6):513; special Issue: Micromechanics of Materials. doi:10.1016/j.ijengsci.2008.01.006
21. Němeček J, Šmilauer V, Kopecký L (2011) Cem Concr Compos 33(2):163
22. Perera D, Uchida O, Vance E, Finnie K (2007) J Mater Sci 42(9):3099. doi:10.1007/s10853-006-0533-6
23. Zaoui A (2002) J Eng Mech 128(8):808
24. Mori T, Tanaka K (1973) Acta Metall 21(5):1605
25. Hill R (1965) J Mech Phys Solids 13:189
26. Palomo A, Grutzeck MW, Blanco MT (1999) Cem Concr Res 29:1323
27. Provis JL, van Deventer JSJ (2007) Chem Eng Sci 62:2318
28. Rodríguez E, de Gutiérrez RM, Bernal S, Gordillo M (2009) Rev Fac Ing 49:30
29. Strnad T (2011) PhD thesis, Faculty of Civil Engineering, Czech Technical University (in Czech)
30. Rahier H, Denayer JF, van Mele B (2003) J Mater Sci 38:3131. doi:10.1023/A:1024733431657
31. Powers TC (1958) J Am Ceram Soc 41(1):1
32. Duxson P, Provis JL, Lukey GC, Mallicoat SW, Kriven WM, van Deventer JSJ (2005) Colloids Surf A 269:47
33. Scherer GW (1999) Cem Concr Res 29(8):1149
34. Constantinides G, Ulm FJ (2007) J Mech Phys Solids 55:64
35. Jennings HM (2008) Cem Concr Res 38(3):275
36. Wongpa J, Kiattikomol K, Jaturapitakkul C, Chindaprasirt P (2010) Mater Des 31(10):4748
37. Matsunaga T, Kim JK, Hardcastle S, Rohatgi PK (2002) Mater Sci Eng A 325(1–2):333
38. van Deventer J, Provis J, Duxson P, Lukey G (2007) J Hazard Mater 139(3):506
39. Neubauer CM, Jennings HM, Garboczi EJ (1997) Cem Concr Res 27(10):1603
40. Neville AM (1997) Properties of concrete. Wiley, New York
41. Šmilauer V (2011) Multiscale hierarchical modeling of hydrating concrete. Saxe-Coburg Publications, Stirling
42. Chen C, Gong W, Lutze W, Pegg I (2011) J Mater Sci 46(9):3073. doi:10.1007/s10853-010-5186-9
43. Duxson P, Mallicoat SW, Lukey GC, Kriven WM, van Deventer JSJ (2007) Colloids Surf A 292(1):8
44. Kirschner AV, Harmuth H (2004) Ceram-Silik 48(3):117
45. Barbosa VFF, MacKenzie KJD, Thaumaturgo C (2000) Int J Inorg Mater 2(4):309